polysaccharides

MDPI

Article

Improving the Corrosion Resistance of Titanium by PAA/Chitosan Bilayer Architecture Through the Layer-by-Layer Method

Daniele Morais Dias [1], Murilo Oliveira Alves Ferreira [2], Ana Paula Ramos [3], Witor Wolf [2], Jéferson Aparecido Moreto [2] and Rodrigo Galo [1,*]

[1] Department of Dental Materials and Prosthesis, School of Dentistry of Ribeirão Preto, University of São Paulo (USP), Ribeirão Preto 14040-904, SP, Brazil; danielemoraisd@usp.br
[2] Materials Engineering Department, São Carlos School of Engineering, University of São Paulo (USP), São Carlos 05508-220, SP, Brazil; moaferreira@usp.br (M.O.A.F.); witorw@usp.br (W.W.); jamoreto@usp.br (J.A.M.)
[3] Department of Chemistry FFCLRP, University of São Paulo (USP), Ribeirão Preto 14040-901, SP, Brazil; anapr@ffclrp.usp.br
* Correspondence: rogalo@forp.usp.br; Tel.: +55-16-3315-3973

Abstract

To enhance interaction with the host tissue and protect the metal surface, various surface treatments can be applied to dental implants. This study aimed to produce layer-by-layer (LbL) films by alternated immersion of the titanium sample into polyacrylic acid (PAA) and chitosan solutions, obtaining a PAA/chitosan bilayer architecture, seeking to improve the corrosion resistance. For this purpose, 03 experimental groups (n = 05) were performed: Ti-Cp (as control), Ti-Cp+8 bilayers PAA/chitosan, and Ti-Cp+12 bilayers PAA/chitosan. The corrosion behavior was assessed by using open-circuit potential (OCP), potentiodynamic polarization curves (PPcs) and electrochemical impedance spectroscopy (EIS) techniques, conducted in 0.9 wt% NaCl solution at a controlled temperature of 25 ± 1 °C. The samples were characterized morphologically and structurally by atomic force microscope (AFM), scanning electron microscopy/energy-dispersive X-ray (SEM/EDX), and X-ray diffraction (XRD) techniques before and after the corrosion tests. The electrochemical results significantly highlight the beneficial influence of coatings based on PAA/chitosan in enhancing the corrosion resistance of titanium. These findings not only corroborate the feasibility of using alternative materials for the protection of titanium but also open new possibilities for the development of innovative coatings that can be applied within the biomedical sector, serving as mediators for medicinal purposes, particularly in osteoconductive interventions.

Keywords: corrosion; titanium; PAA/chitosan coatings; dental implant; surface treatment

Academic Editor: Karin Stana Kleinschek

Received: 19 April 2025
Revised: 26 May 2025
Accepted: 27 June 2025
Published: 1 July 2025

Citation: Dias, D.M.; Ferreira, M.O.A.; Ramos, A.P.; Wolf, W.; Moreto, J.A.; Galo, R. Improving the Corrosion Resistance of Titanium by PAA/Chitosan Bilayer Architecture Through the Layer-by-Layer Method. *Polysaccharides* **2025**, *6*, 57. https://doi.org/10.3390/polysaccharides6030057

1. Introduction

The use of dental implants is one of the most reliable methods for replacing lost dental elements [1]. The implant's success hinges upon the interaction of the material with the host bone tissue, which is initially dictated by the composition and topography of the surfaces [2–4]. Therefore, commercially pure titanium (Ti-Cp) and its alloys are the most used materials in the manufacture of dental implants, since they bear suitable mechanical properties, high corrosion resistance, and adequate biocompatibility [5–8]. The good corrosion resistance of titanium and its alloys arises from the thin TiO_2 layer that spontaneously forms on their surface when exposed to the atmosphere [9,10]. However, the Ti by itself is not capable of preventing long-term corrosion when installed in the oral

cavity. The challenging environment, linked to the impact of masticatory forces capable of inducing mechanical wear in the contact zone, exerts a profound influence on the chemical, as well as the mechanical conditions of this metal [11].

Although Ti-Cp possesses inherent corrosion resistance, the dynamic oral environment (pH fluctuations between 2.0 and 7.8, cyclic masticatory forces up to 70 N, and bacterial biofilms) can locally compromise the TiO_2 passive layer [5,12]. As Mathew et al. [13] demonstrated, this localized degradation triggers the release of pro-inflammatory Ti^{4+} ions, justifying additional protective strategies.

The chemical degradation still compromises the tribological properties of Ti [14,15], thus promoting the release of by-products from deterioration of the material around adjacent tissues [16,17]. This process can be correlated to ineffective osseointegration and implant failure caused by infections, osteolysis, and bone resorption [18]. To address these challenges, surface modification of titanium through chemical or physical texturing has been employed as a strategic approach to enhance both the biological response and the fixation of dental implants compared to unmodified titanium surfaces [19,20]. Therefore, the main objectives in implantology are increasing the success rate of dental implants by tuning surface properties, stimulating osseointegration, and reducing the healing period [21].

Some methods can be cited, including blasting and chemical treatment. Blasting is responsible for the increased adhesion of odontoblastic cells [22]. Chemical treatment, using either hydrogen peroxide or hydrochloric acid (HCl), triggers new bone formation through apatite deposition and forming a layer of bioactive Ti-gel on complex surfaces [23]. Furthermore, chitosan/polyacrylic acid multilayers deposited by the layer-by-layer (LbL) technique promote adhesion, proliferation, and differentiation of bone cells on the Ti surface, which might improve osseointegration and antibacterial properties of the implants [24]. Moreover, the coatings can improve responses against chemical degradation, since they avoid direct contact between the corrosive environment from body fluids and the substrate [25,26].

Chitosan, a cationic biopolymer obtained through the deacetylation of chitin, has been employed as a biomaterial for the surface texturing of titanium [27]. Among its advantageous attributes, chitosan can activate macrophages and neutrophils, stimulate fibroblastic cell activity, detect growth factors, and trigger the production of cytokines and collagen. Additionally, it plays a pivotal role in activating angiogenesis processes [28]. Using chitosan can enhance the contact between the surface of the implant and the host bone tissue by changing the modulus of elasticity, thus reducing the mismatch between the interfaces, decreasing areas of stress concentration [29]. Moreover, the functional groups of chitosan can bind different molecules and act as a carrier of bioactive molecules, such as antibiotics, for site-specific delivery around the implant area [30]. Changing the implant surface chemistry can increase bioactivity and corrosion resistance; therefore, chitosan films can be a promising protection against the natural deterioration in the oral environment [31]. Unlike prior studies focusing exclusively on either bioactivity or corrosion resistance [32,33], the present work introduces a dual-functional multilayer system that (i) reduces electrochemical degradation of the Ti-Cp substrate to below critical thresholds associated with peri-implantitis (<1 $\mu A/cm^2$) [34] and (ii) maintains osteoconductivity through the carboxyl functional groups of PAA.

In this study, we present an innovative and applied research effort to demonstrate the feasibility of Ti-Cp functionalization by applying multiple layers of chitosan using the layer-by-layer (LbL) methodology. Subsequently, the investigation sought to determine whether the resultant coating influences the ability of Ti-Cp surfaces to resist chemical degradation when exposed to a saline solution.

2. Materials and Methods

2.1. Specimen Preparation

Discs (Ø13 × 2 mm) composed of machined commercially pure titanium (Dentaurum, Inspringen, Germany) were used in the present work. Before the electrochemical tests, the samples underwent metallographic preparation and were sanded using silicon carbide (SiC) sandpapers in the sequence range of 240, 400, 600, 800, 1200, and 2000 mesh. The polishing process was carried out using diamond paste down to 1 µm (Strues, Glasgow, UK), 0.06 µm diameter colloidal silica particles, and 0.05 µm diameter alumina particles (Strues, Glasgow, UK), and finished with a cloth wheel and OSP solution (Colloidal silica suspension—SiO_2—0.04 µm) + 30% H_2O, following the recommendations described by Caio et al. [35]. The sanding and polishing processes were conducted using FORTEL/PFL model equipment at an angular frequency of 600 rpm. Last, the samples were ultrasonically cleaned for 10 min in propanol and 5 min in distilled water. The samples were kept for 14 h in a desiccator to obtain similar surface conditions.

2.2. Deposition of the Chitosan/PAA Coating on Ti-Cp

Initially, an aqueous solution of chitosan and PAA was prepared. For this, 2.5 mL of acetic acid (Glass-Lab) and 0.25 mg of chitosan were added to 250 mL of water from a Milli-Q® system. In another beaker, 0.5 g of PAA was dissolved in 250 mL of water from a Milli-Q® system [36]. The solutions were heated to 60 °C, with continuous stirring, for 4 h, followed by an additional 24 h at room temperature. Subsequently, the solutions were filtered through a 0.45 µm pore filter (JET BIOFIL®, Guangzhou Jet, Guangzhou, China), employing a 10 mL syringe for assistance. LbL assembly was executed through the sequential deposition of PAA and chitosan onto the Ti discs at a pH of 3.5. Employing a dip-coater, the Ti-Cp disc was immersed in a solution containing the polyanion PAA for 20 min to facilitate the deposition of the initial layer. Subsequently, washing was conducted to eliminate loosely bound or unbound polyelectrolyte chains by immersing the sample in Milli-Q water for 5 min. This step is characterized by avoiding cross-contamination of polyelectrolytes with opposite charges. The Ti-Cp disc containing the first PAA layer was immersed in the solution containing the polycation chitosan for 20 min. The discs were dried with an air jet between each deposition. This process was repeated until the desired layers were achieved. In this study, we prepared Ti-coated samples containing 8 and 12 layers of the polyelectrolytes. The immersion times were selected based on adsorption kinetics studies for PAA and chitosan, where 20 min ensures complete and homogeneous layer coverage, and 5 min is sufficient for rinsing without destabilizing the multilayer structure [36–38]. Figure 1 shows a schematic setup of PAA/chitosan LbL film fabrication onto titanium (top), followed by digital photography of the film (geometric area of 1.5 cm^2) with different numbers of bilayers (bottom). It is very important to emphasize that the drying process was performed by using a nitrogen jet.

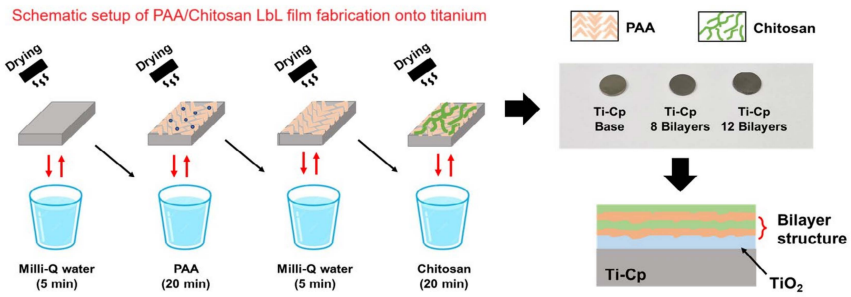

Figure 1. Schematic setup of PAA/chitosan LbL film fabrication onto titanium (**top**), followed by digital photography of the film (geometric area of 1.5 cm^2) with different numbers of bilayers (**bottom**). The drying process was carried out using a nitrogen jet.

2.3. Corrosion Tests

In this study, we examined the impact of bilayers deposited onto Ti-Cp specimens through the LbL method by using uniform electrochemical tests. For this purpose, open-circuit potential (OCP), potentiodynamic polarization curves (PPcs), and electrochemical impedance spectroscopy (EIS) tests were performed in 0.9 wt% NaCl solution at room temperature. The electrochemical tests were performed by using a μStat-i 400s/MetrOhm potentiostat/galvanostat (DropSens, Metrohm, Oviedo, Spain) and an electrochemical cell containing a three-electrode compartment, consisting of a working electrode with an exposed area of 1 cm^2 (samples of Ti-Cp with and without PAA/chitosan), a platinum (Pt) counter electrode, and a saturated calomel reference electrode (SCE) (Hg/Hg_2Cl_2, KCl_{sat}), at the Department of Materials Engineering (SMM) of the São Carlos School of Engineering (EESC) at the University of São Paulo (USP), São Carlos, São Paulo, Brazil. The samples' corrosion potential (E_{OCP}) was monitored during 1 h (3600 s). The PPc tests started at −0.5 V versus E_{OCP} in the anodic direction up to 2.0 V/SCE, with a sweep rate of 1 mV s^{-1}. The EIS spectra were recorded over a frequency range of 100 kHz to 10 mHz, employing a sinusoidal wave of 10 mV (rms). EIS spectra were obtained for at least three samples of each specimen (3 h, 12 h, 24 h, and 48 h of immersion), and the consistency of the impedance data and compliance with validation criteria for these measurements were assessed using the Kramers–Kronig (KK) transformations. The corrosion micromechanisms associated with each sample type were elucidated using equivalent electrical circuits (EECs) through the Zview2 software version 2.9b.

2.4. Morphological and Structural Characterization

The morphology and composition of the Ti-Cp and Ti-Cp containing chitosan bilayers were assessed by scanning electron microscopy (SEM) and energy-dispersive X-ray spectroscopy (XRD) techniques, before and after the corrosion tests. For this purpose, SEM analyses were carried out by using ZEISS EVO Family Modular SEM Platform equipment (Carl Zeiss Microscopy GmbH, Oberkochen, Germany) at the Medicine School, University of São Paulo (USP), Ribeirão Preto, SP, Brazil. These analyses were performed on all samples before and after the potentiodynamic polarization tests. The surface morphology of the Ti-Cp, Ti-Cp+8 bilayer and Ti-Cp+12 bilayer samples was also evaluated following the EIS tests. Micrographs were acquired using a secondary electron (SE) detector. For this purpose, a FEI Inspect S50 scanning electron microscope equipped with a tungsten electron gun, operating at 20 kV, was utilized in the Materials Engineering Department (DEMA) at the Federal University of São Carlos (UFSCar), São Carlos, SP, Brazil. The AFM analyses were performed using a FlexAFM NanoSurf equipment (Nanosurf AG, Liestal, Switzerland) at the Chemical Department at the Faculty of Philosophy, Sciences and Letters of Ribeirão Preto, SP, Brazil, operating in dynamic mode, with an acquisition speed of 0.25 Hz to 1 Hz, with a C300 controller (Nanosurf AG, Liestal, Switzerland). The images were processed using the Gwyddion program. XRD diffractograms were obtained by using a PANalytical model X'Pert PRO MPD diffractometer, under CuKα radiation. Measurements were carried out using the grazing incidence X-ray diffraction technique (GID) on the incident angle fixed at 6°. A high-resolution PIXcel 1D semiconductor radiation detector scanned the diffracted radiation, rotating between 5 and 80° (2θ), with an angular step of 0.0263° and a 80 s counting time per point. The voltage and current used were 40 kV and 30 mA, respectively.

3. Results and Discussion

In this study, uniform electrochemical tests were conducted to explore the impact of PAA/chitosan coating on the corrosion resistance of Ti-Cp alloy. Figure 2a displays representative curves depicting the evolution of the open-circuit potential over time for

the Ti-Cp with and without chitosan bilayers, whilst Figure 2b exhibits the characteristic potentiodynamic polarization curves. The results indicate that the open-circuit potential (E_{ocp}) values for the Ti-cp specimen incorporating 12 chitosan bilayers were shifted towards less negative values. This shift suggests enhanced surface protection and possibly improved resistance to corrosion processes. In contrast, the samples of Ti-Cp and those with eight chitosan bilayers exhibited quite similar electrochemical behavior. As can be seen, the alloy with Ti-Cp+12 bilayers exhibits a corrosion potential (Ei = 0) that is slightly more positive than that measured in the Ti-Cp and Ti-Cp+8 bilayers. As reported in the literature [39–45], the value of corrosion potential (Ecorr) is typically regarded as an indicator of the nobility of the material; a higher E_{corr} corresponds to a more corrosion-resistant system. The beneficial effect of the coating is also evidenced by the i_{corr} values, which demonstrate a significant reduction. This improvement can be attributed to the shift of the cathodic branch of the coated samples, which is positioned further to the left in the curve presented in Figure 2b. This shift indicates a decrease in the corrosion rate, suggesting that the coating effectively protects against corrosion, resulting in superior electrochemical performance. Thus, it is evident that the coating application not only enhances corrosion resistance but also modifies the dynamic characteristics of the interface between the material and the corrosive medium, thereby offering even more robust protection for the analyzed samples. These results highlight the importance of selecting suitable coatings to enhance the durability and structural integrity of materials exposed to harsh environments.

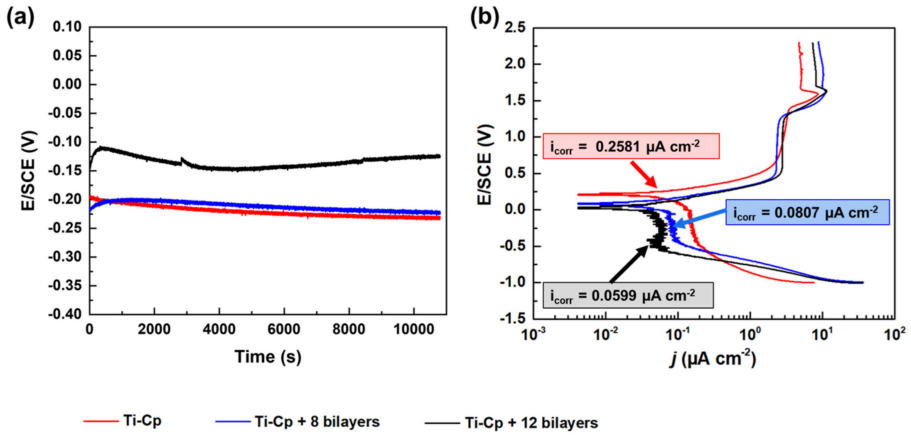

Figure 2. (**a**) Open-circuit potential variation with time and (**b**) characteristic potentiodynamic polarization curves for the Ti-Cp with and without chitosan bilayers in aerated 0.9% NaCl solution.

Figure 3a–f displays the SEM images and the XRD spectrum before and after the potentiodynamic polarization tests for Ti-Cp, Ti-Cp+8 bilayers, and Ti-Cp+12 bilayers. As is evident, deposits form noticeably on the surface of the Ti-Cp+8 bilayer and discreetly on both the base material and Ti-Cp + 12 bilayers. As observed in the XRD patterns, there are no discernible structural differences between the specimens before and after undergoing corrosion electrochemical tests. Conversely, the absence of additional peaks following the deposition of PAA/chitosan on the Ti-Cp surfaces suggests the formation of amorphous layers. The 2D and 3D morphological projections obtained using the AFM technique are depicted in Figure 4. The 3D morphological projections acquired with AFM showed a gradual quantitative increase in the roughness of the Ti-Cp sample (166.09 nm to 338.11 nm) and Ti-Cp+8 layers of PAA/chitosan (143.90 nm to 261.48 nm) after the corrosion assays. However, for the Ti-Cp+12 layers of PAA/chitosan, the roughness decreased after electrochemical assays (118.37 nm to 104.17 nm). Concerning the Ti-Cp+12 layers of the PAA/chitosan specimen, this modification may have occurred due to corrosion products'

sealing of defect regions. Further discussions can be made with the EIS analyses in the following paragraphs.

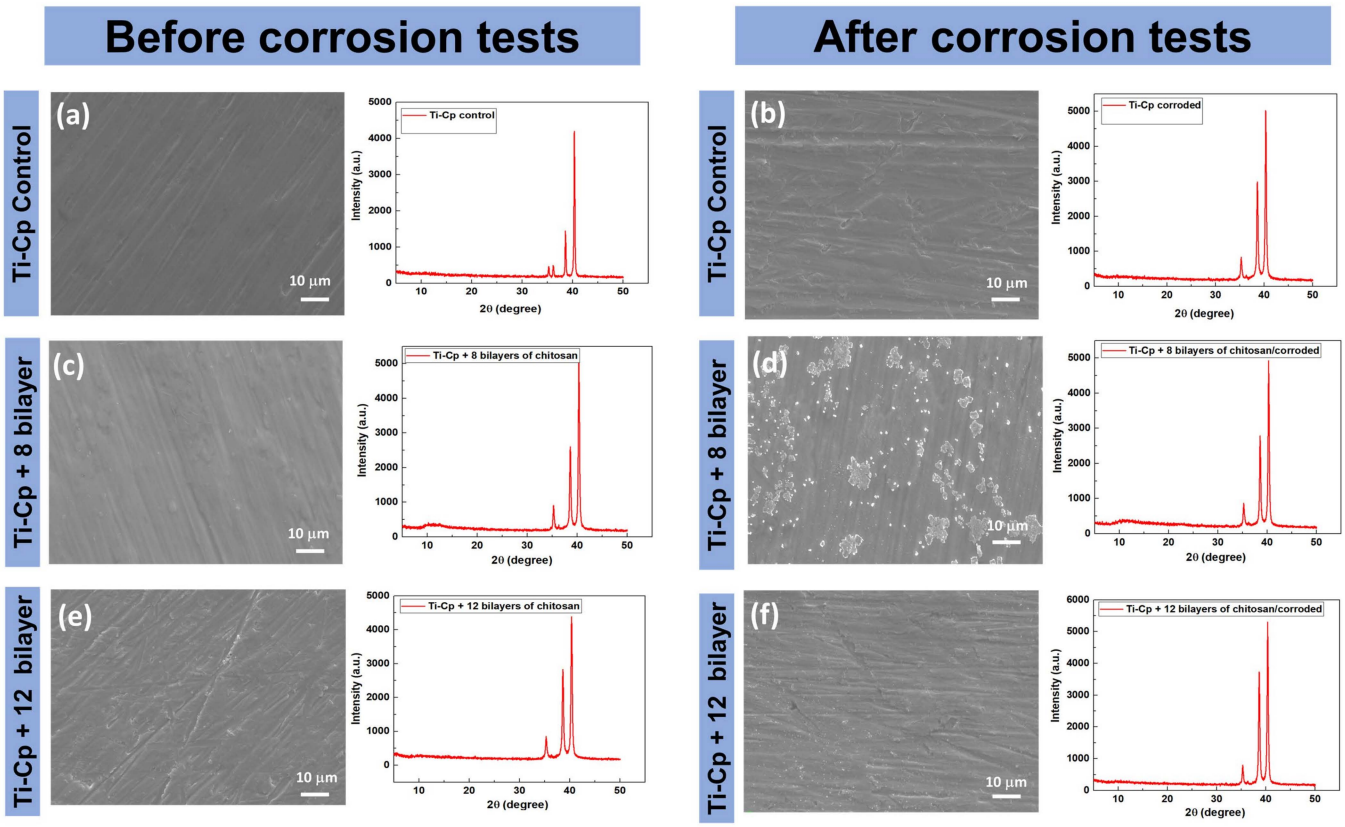

Figure 3. SEM images obtained using secondary electrons (SE) mode and X-ray diffraction patterns for the (**a**) Ti-Cp without corrosion test, (**b**) Ti-Cp after corrosion tests, (**c**) Ti-Cp+8 bilayers before corrosion tests, (**d**) Ti-Cp+8 bilayers after corrosion tests, (**e**) Ti-Cp+12 bilayers before corrosion tests, and (**f**) Ti-Cp+12 bilayers after corrosion tests.

The observed increases in film thickness, congruent with previously reported values for polyacrylic acid (PAA)/chitosan bilayers in the literature [37,38], coupled with the surface morphology (as evidenced by SEM and AFM analyses) and the substantial enhancement in electrochemical impedance moduli, collectively furnish compelling evidence for the efficacious formation of the self-assembled multilayer coating. These multifaceted parameters are widely acknowledged in the scientific community as robust and reliable indicators of successful LbL film construction [37,45]. The convergence of these multiple lines of evidence substantiates the integrity and consistency of the fabricated nanostructured coating, thereby corroborating the effectiveness of the employed LbL assembly methodology.

Figure 5 presents the Bode plots and Nyquist diagrams for the Ti-Cp and Ti-Cp samples with 8 and 12 bilayers, analyzed over various immersion times. These diagrams provide a clear insight into the electrochemical properties of the samples, enabling the assessment of changes in impedance over time. By analyzing these data, it becomes possible to discern the influence of the number of bilayers on each sample's electrochemical behavior and corrosion resistance, thereby facilitating a deeper understanding of the mechanisms involved in the interactions between the surfaces and the corrosive medium. A general analysis of the impedance spectra reveals the presence of two time constants: one at high frequencies and the other at low frequencies, as well as the chitosan coatings' positive influence in improving the Ti-Cp's corrosion resistance for all immersion times studied.

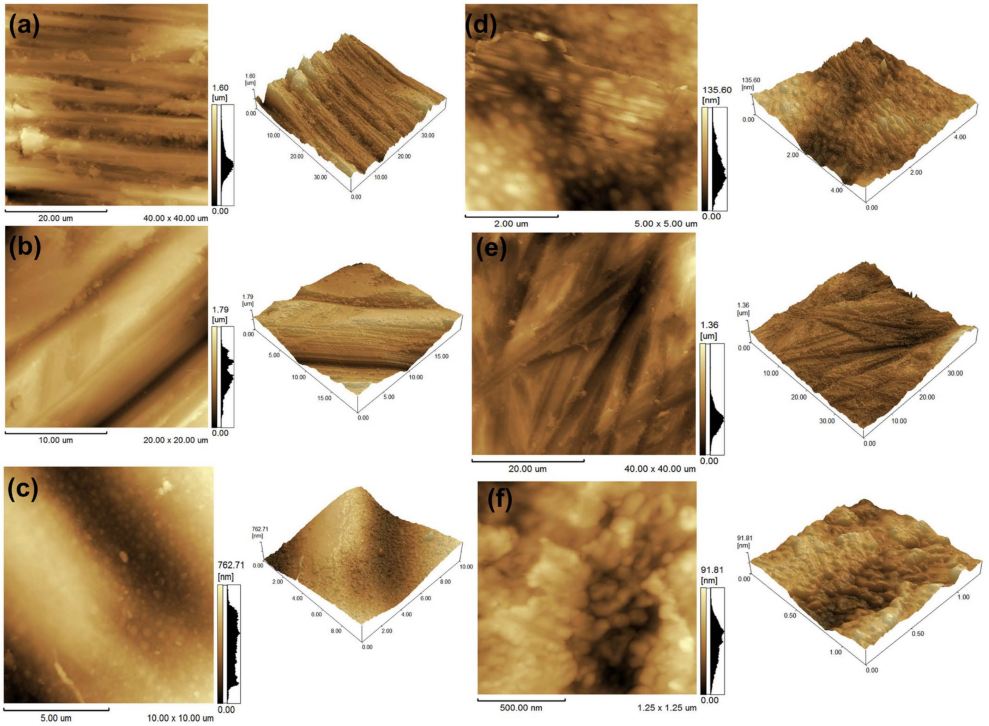

Figure 4. Two- and three-dimensional morphological projections obtained by using AFM technique for the (**a**) Ti-Cp without corrosion test, (**b**) Ti-Cp after corrosion tests, (**c**) Ti-Cp+8 bilayers before corrosion tests, (**d**) Ti-Cp+8 bilayers after corrosion tests, (**e**) Ti-Cp+12 bilayers before corrosion tests, and (**f**) Ti-Cp+12 bilayers after corrosion tests.

The present work proposes two equivalent electrical circuits (EECs) to elucidate the corrosion mechanisms involved. The first one (see Figure 6a), referred to as EEC1 [46], was proposed for the Ti-Cp specimens and consists of the Ohmic resistance (R_Ω) and the loop CPE_{bl}-R_{bl}, which represents the constant phase element of the barrier layer and its resistance.

The Ohmic resistance, denoted as R_Ω, is the sum of the resistance of the electrolyte (R_s), the resistance of the electrical wires ($R_{el,w}$), and the internal resistance of the electrodes ($R_{int,el}$). Generally, the latter two terms are negligible in comparison to the first. Thus, for a region defined by an area (A) and a length (l), traversed by a uniform electric current, R_s can be expressed as follows: $R_s = \rho\ (l/A)$, where ρ represents the electrical resistivity in $\Omega\ m^{-1}$. The EEC2 [34] presented in Figure 6b was employed to describe the corrosion properties of the chitosan bilayer samples. In this circuit, R_s represents the resistance of the solution, with the loop CPE_{bl}-R_{bl} associated with the inner layer, and the loop CPE_p-R_p corresponding to the outer layer. The impedance of a constant phase element, Z_{CPE}, can be expressed as ($Z_{CPE} = 1/[Y_0(j\omega)^n]$, where $-1 \leq n \leq 1$. The values of the parameter n are directly related to the non-uniform distribution of electric current over the surface of the working electrode, which arises due to the presence of roughness and defects. Consequently, for heterogeneous surfaces, the values of n become less than 1, and Y_0 does not represent capacitance. In the context of this study, the most critical aspect is not merely the precise determination of capacitance values, but rather the understanding of the corrosion mechanisms involved. In this sense, constant phase elements will be interpreted as indicative of capacitance.

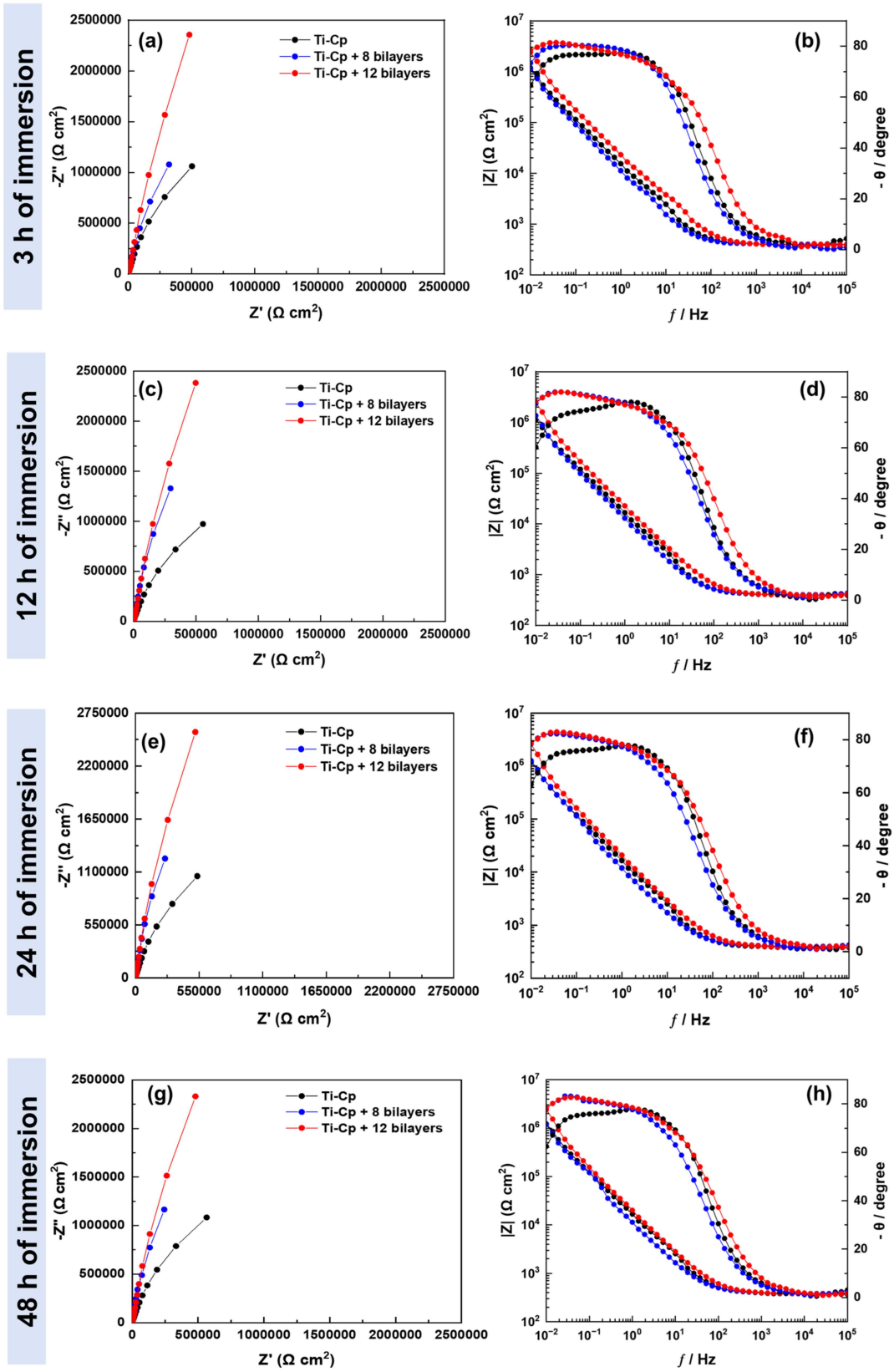

Figure 5. Nyquist plots (**a**,**c**,**e**,**g**) and Bode plots (**b**,**d**,**f**,**h**) of electrochemical impedance spectra for Ti-Cp, Ti-Cp+8 bilayers, and Ti-Cp+12 bilayers after 3, 12, 24, and 48 h of immersion in aerated 0.9% NaCl solution. The multilayer coatings improved corrosion resistance over time.

Figure 7 presents a compilation of the results obtained from the fittings of the EIS data for the Ti-Cp samples, Ti-Cp+8 layers, and Ti-Cp+12 layers, respectively. As previously

mentioned, two EECs were utilized to elucidate the corrosion mechanisms of the samples with and without coating. In this sense, Figure 7 displays the obtained parameters from the fitting and demonstrates the corrosion behavior with immersion time for the compact barrier and the outer chitosan layers (8 and 12 bilayers). It is observed that, across all the samples analyzed, the electrolyte resistance remains virtually constant throughout all immersion times. This behavior was anticipated, as the distance between the working and reference electrodes was kept constant during the execution of the electrochemical corrosion tests. Moreover, considering that the maximum immersion period evaluated was 48 h, there was no significant evaporation of the solution that might have introduced variations into the results obtained. This stringent control of experimental conditions ensures that any variations observed in the data are not due to environmental changes but are intrinsic to the material characteristics of the samples under study. The capacitance behavior of the barrier layer demonstrates remarkable stability across all immersion periods for the Ti-Cp sample. This consistency signifies effective protection of the titanium surface against corrosion, reflecting both the integrity of the coating and the efficacy of the TiO_2 layer formation at the interface. In comparing the capacitance values between the Ti-Cp+8 bilayers and the Ti-Cp+12 bilayers samples, it is evident that the latter exhibits significantly lower capacitance values throughout the entire testing duration. This observation suggests that the additional bilayers may contribute to a denser and more effective barrier against corrosive processes, enhancing the overall protective performance of the coating. Considering that the capacitance of the inner layer may be written as $C_{bl} = (\kappa\varepsilon_0 A)/d$, where ε_0 is the vacuum permittivity (8.85 pF/m), κ represents the dielectric constant of the oxide film, A is the sample surface area, and d the thickness, and assuming that the surface area of the oxide is kept almost constant upon immersion and that the same applies to the oxide thickness, the continuous increase of the capacitance values may only be explained based on the change of the dielectric constant [47]. The values of C_{bl} align with those obtained for the resistance of the barrier layer. Lastly, the values of n_{bl} range from 0.88 to 0.98.

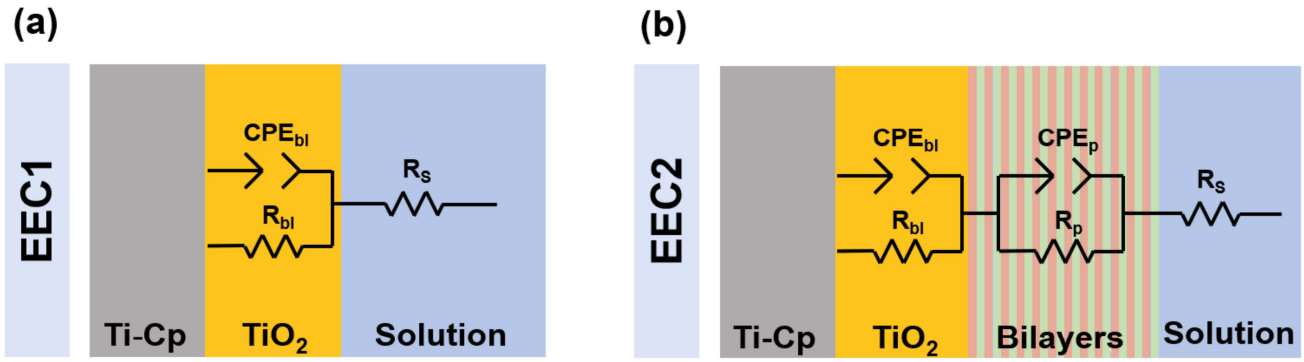

Figure 6. Schematic representation of the corrosion and the proposed equivalent circuit: (**a**) EEC1 for the Ti-Cp sample, and (**b**) EEC2 for the Ti-Cp+8 bilayers and Ti-Cp+12 bilayers.

Upon examining the results obtained for the coated specimens, it is observed that the capacitance values of the outer layer, C_p, are significantly higher in the Ti-Cp+8 bilayers sample. In this case, the increase in C_p values over the immersion time may be associated with an enhancement in the electroactive area or a reduction in the thickness of the chitosan film deposited on the sample's surface. Thus, it can be inferred that the sample containing 12 bilayers exhibits a superior resistance to the corrosion process. This enhanced performance may be attributed to the effective barrier properties offered by the additional bilayers, which likely improve the protective capabilities of the coating against corrosive agents. The increased bilayers may contribute to a more uniform and dense structure, thereby minimizing the penetration of corrosive species and maximizing the underlying sample's

electrochemical protection. The results for C_p align closely with the values of outer layer resistance for the sample with eight bilayers. The sample containing 12 bilayers increased the R_p values, starting from the first 3 h of immersion in a 0.9% NaCl solution. These values remained approximately constant until the conclusion of the corrosion testing. Therefore, considering that R_p can be expressed as $R_p = R_p$ ($A_{geometric}/A_{corroded}$), the observed increase with immersion time is attributed to forming a surface layer of corrosion products. This layer plays a crucial role in sealing the defects present on the sample surface, thereby enhancing the overall protective properties of the coating. The gradual accumulation of corrosion products suggests that the sample experiences self-healing, which improves corrosion resistance over time. Concerning the n_p parameter, it is evident that the Ti-Cp+8 bilayer sample displays values ranging from 0.66 to 0.76, whereas the Ti-Cp+12 bilayer sample presents values between 0.70 and 0.80. These findings suggest that the surface comprising 12 bilayers is more homogeneous, a conclusion that is consistent with the surface roughness measurements obtained through AFM analyses. Figure 8 exhibits the Bode plots and Nyquist diagrams of EIS spectra and fitting of Ti-Cp, Ti-Cp+8 bilayers, and Ti-Cp+12 bilayers exposed to 0.9 wt% NaCl solution, corresponding to the mathematical modeling of these data using equivalent electrical circuits (EECs). Thus, the impedance spectra were fitted to these circuits, resulting in an excellent correlation, with x^2 values in the range of 10^{-4}. Figure 9 presents images acquired using SEM/EDX techniques, depicting the surfaces of both coated and uncoated samples after the execution of EIS measurements. The analyses distinctly reveal variations in surface morphology between the samples, highlighting the modifications introduced by applying the PAA/chitosan coating. The EDX analyses were adequately sufficient to confirm the presence of the characteristic chemical elements of polyacrylic acid (PAA) and chitosan, respectively.

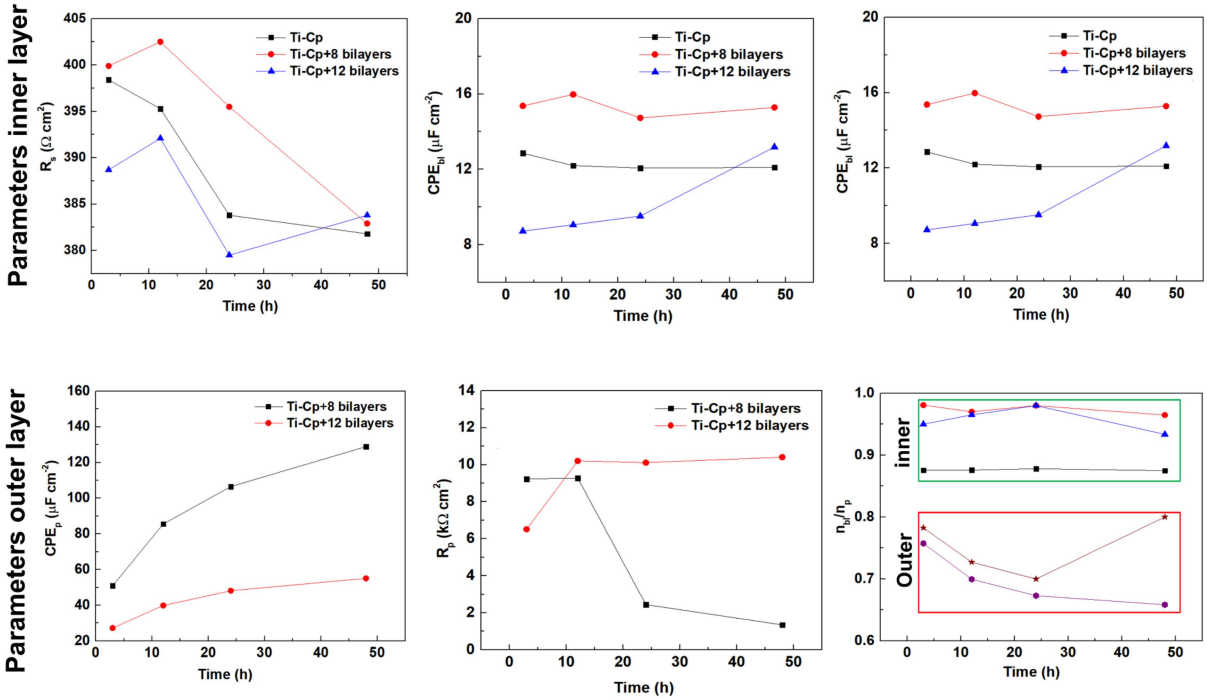

Figure 7. Average values of the EIS parameters of Ti-Cp, Ti-Cp+8 bilayers, and Ti-Cp+12 bilayers after exposure to 0.9 wt% NaCl solution. Green: Ti-Cp+8 bilayers (inner layer); Red: Ti-Cp+12 bilayers (outer layer).

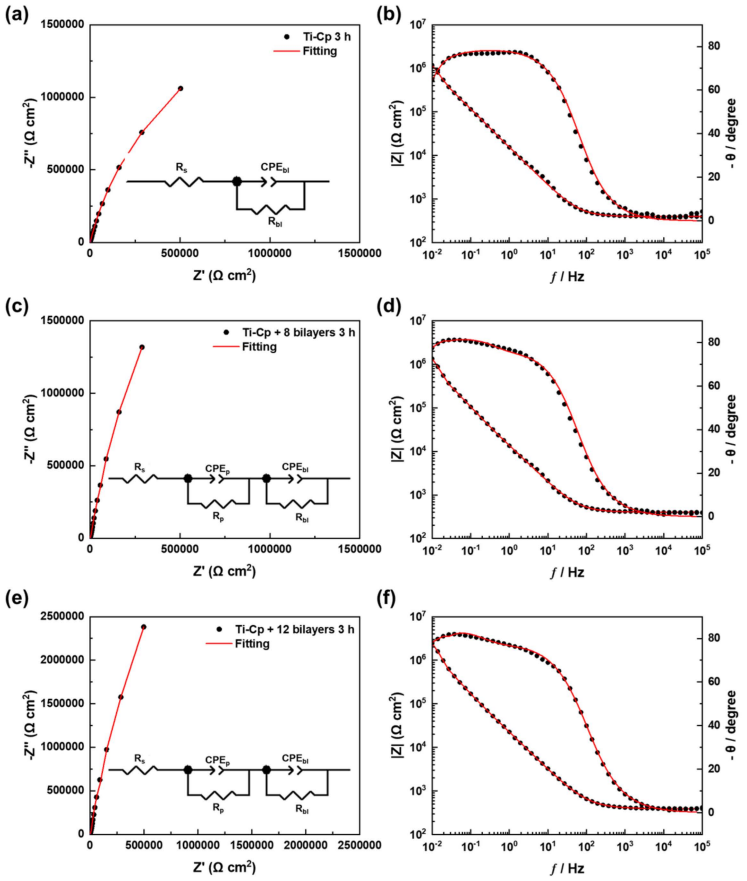

Figure 8. Nyquist (**a**,**c**,**e**) and Bode (**b**,**d**,**f**) plots of EIS spectra and fittings for Ti-Cp (**a**,**b**), Ti-Cp + 8 bilayers (**c**,**d**), and Ti-Cp + 12 bilayers (**e**,**f**) after 3 h of immersion in 0.9% NaCl solution. Black dots represent experimental data, and red lines indicate the fitting curves.

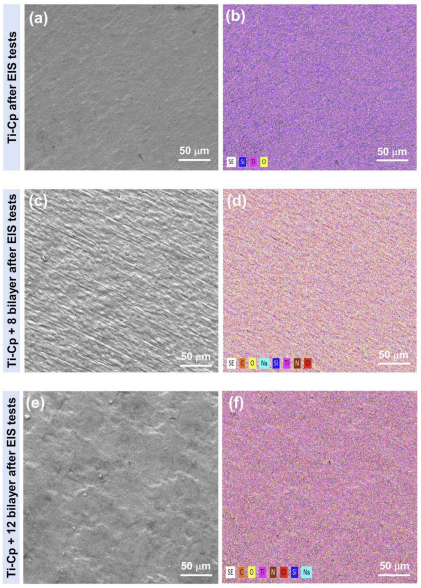

Figure 9. SEM/EDX images of the surfaces of coated and uncoated samples after EIS measurements in 0.9 wt% NaCl solution: (**a**,**b**) Ti-Cp; (**c**,**d**) Ti-Cp + 8 bilayers; (**e**,**f**) Ti-Cp + 12 bilayers.

Considering the electrochemical results, a corrosion mechanism may be proposed (see Figure 10). Since the coatings are manually applied to the Ti-Cp surfaces using the LbL technique, ensuring uniformity in forming these layers is challenging. This variability is likely attributable to numerous agglomerates observed across different regions of the surfaces

that contain immobilized PPA/chitosan. When the functionalized material is subjected to a corrosive medium containing Cl^- ions, an electrostatic attraction is established between the positive charges of chitosan and the negatively charged ions present in the solution. This interaction may facilitate localized corrosion processes, as the heterogeneity of the coating can lead to differential responses in various surface areas. Consequently, understanding the interplay between agglomerates and the electrochemical behavior in the chloride-rich environment becomes crucial for assessing the durability and efficacy of the coatings.

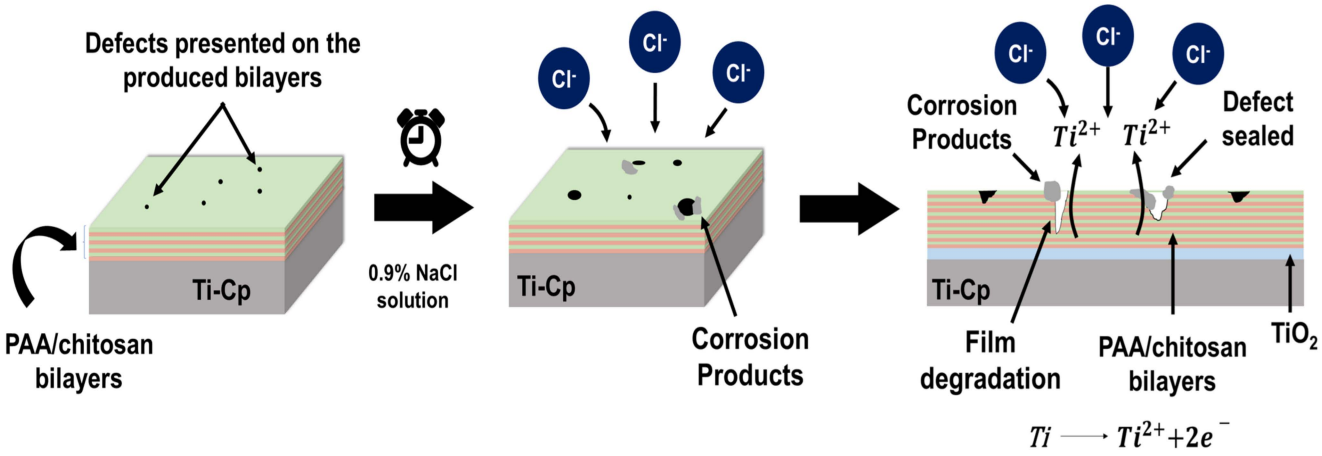

Figure 10. A corrosion mechanism was proposed for the Ti-Cp+8 and Ti-Cp+12 bilayers after EIS tests in 0.9% NaCl solution.

4. Conclusions

The primary objective of this study was to evaluate the influence of PAA, and chitosan coatings applied to the surface of titanium via the LbL technique. Corrosion tests conducted on both coated and uncoated specimens demonstrated that using 8 and 12 bilayers significantly enhanced the electrochemical performance of the titanium substrates. Specifically, these coatings yielded markedly lower corrosion current density values, 0.2581 $\mu A/cm^2$ (Ti-Cp), 0.0807 $\mu A/cm^2$ (Ti-Cp+8 bilayer), and 0.0599 $\mu A/cm^2$ (Ti-Cp+12 bilayer); lower corrosion rates, 0.0573 mm/year (Ti-Cp), 0.0179 mm/year (Ti-Cp+8 bilayer), and 0.0132 mm/year (Ti-Cp+12 bilayer); and higher impedance moduli compared to the uncoated base material across all immersion durations assessed. Furthermore, it is noteworthy that, besides enhancing titanium's anticorrosive properties, chitosan exhibits potential as a mediator for medicinal applications, particularly in promoting osteoconductive activities. This dual functionality underscores the versatility of PAA/chitosan coatings, paving the way for their use in sophisticated biomedical applications where both corrosion resistance and biocompatibility are imperative.

Author Contributions: D.M.D., investigation and writing; M.O.A.F., investigation and formal analysis; A.P.R., investigation and formal analysis; W.W., investigation and formal analysis; Moreto, J.A.M., writing and formal analysis; R.G., supervision, project administration, and formal analysis. All authors have read and agreed to the published version of the manuscript.

Funding: R. Galo would like to acknowledge the financial support received from the São Paulo Research Foundation—FAPESP (Grants 2022/07162-5); and J. A. Moreto would like to acknowledge the financial support received from the National Council for Scientific and Technological Development (CNPq-Brazil) (Grants 303659/2019-0, 402988/2021-3, 302770/2022-4), as well as FAPESP (Grant 2024/02504-0). The authors acknowledge the financial support from CAPES: 001.

Institutional Review Board Statement: Not applicable.

Data Availability Statement: Data are contained within the article.

Acknowledgments: The authors would like to thank the laboratory technicians who helped and enabled the analyses to be carried out, the departments involved, and the entire structure provided by the University of São Paulo (USP), São Paulo State, Brazil.

Conflicts of Interest: The authors declare no conflicts of interest.

References

1. Ashtiani, R.E.; Alam, M.; Tavakolizadeh, S.; Abbasi, K. The Role of Biomaterials and Biocompatible Materials in Implant-Supported Dental Prosthesis. *Evid.-Based Complement. Altern. Med.* **2021**, *5*, 1–9. [CrossRef] [PubMed]
2. Surmenev, R.A.; Surmeneva, M.A.; Ivanova, A.A. Significance of calcium phosphate coatings for the enhancement of new bone osteogenesis–a review. *Acta Biomater.* **2014**, *10*, 557–579. [CrossRef] [PubMed]
3. Ribeiro, A.R.; Oliveira, F.; Boldrini, L.C.; Leite, P.E.; Falagan-Lotcsch, P.; Linhares, A.B.R.; Zambuzzi, W.F.; Fragneaud, B.; Campos, P.C.; Gouvêa, C.P.; et al. Micro-arc oxidation as a tool to develop multifunctional calcium-rich surfaces for dental implant applications. *Mater. Sci. Eng.* **2015**, *54*, 196–206. [CrossRef]
4. Terheyden, H.; Lang, N.P.; Bierbaum, S.; Stadlinger, B. Osseointegration– communication of cells. *Clin. Oral Implant. research* **2012**, *23*, 1127–1135. [CrossRef] [PubMed]
5. Vieira, A.C.; Ribeiro, A.R.L.; Rocha, L.A.; Celis, J.P. Influence of pH and corrosion inhibitors on the tribocorrosion of titanium in artificial saliva. *Wear* **2006**, *261*, 994–1001. [CrossRef]
6. Elias, C.N.; Fernandes, D.J.; Resende, C.R.S.; Roestel, J. Mechanical properties, surface morphology and stability of a modified commercially pure high-strength titanium alloy for dental implants. *Dent. Mater.* **2015**, *31*, e1–e13. [CrossRef]
7. Kulkarni, M.; Flasker, A.; Lokar, M.; Polisak, K.M.; Mazare, A.; Artenjak, A.; Cucnik, S.; Kralj, S.; Velikonja, A.; Iglic, V.K.; et al. Binding of plasma proteins to titanium dioxide nanotubes with different diameters. *Int. J. Nanomed.* **2015**, *10*, 1359–1373.
8. Shibata, Y.; Tanimoto, Y. A review of improved fixation methods for dental implants. Part I: Surface optimization for rapid osseointegration. *J. Prosthodont. Res.* **2015**, *59*, 20–33. [CrossRef]
9. Bronze-Uhle, E.S.; Dias, L.F.G.; Trino, L.D.; Matos, A.A.; De Oliveira, R.C.; Lisboa-Filho, P.N. Physicochemical characterization of albumin immobilized on different TiO2 surfaces for use in implant materials. *Colloids Surf. A Physicochem. Eng. Asp.* **2019**, *564*, 39–50. [CrossRef]
10. López-Valverde, N.; Aragoneses, J.; López-Valverde, A.; Rodríguez, C.; Macedo de Sousa, B.; Aragoneses, J.M. Role of chitosan in titanium coatings trends and new generations of coatings. *Front. Bioeng. Biotechnol.* **2022**, *10*, 907589. [CrossRef]
11. Trino, L.D.; Bronze-Uhle, E.S.; Ramachandran, A.; Lisboa-Filho, P.N.; Mathew, M.T.; George, A. Titanium surface bio-functionalization using osteogenic peptides: Surface chemistry, biocompatibility, corrosion and tribocorrosion aspects. *J. Mech. Behav. Biomed. Mater.* **2018**, *81*, 26–38. [CrossRef] [PubMed]
12. Katić, J.; Šarić, A.; Despotović, I.; Matijaković, N.; Petković, M.; Petrović, Ž. Bioactive Coating on Titanium Dental Implants for Improved Anticorrosion Protection: A Combined Experimental and Theoretical Study. *Coatings* **2019**, *9*, 612. [CrossRef]
13. Mathew, M.T.; Barao, V.A.; Yuan, J.C.; Assunção, W.G.; Sukotjo, C.; Wimmer, M.A. In Situ Corrosion Mapping of Dental Implants. *J. Dent. Res.* **2022**, *101*, 245–253.
14. Fernandes, A.C.; Vaz, F.; Ariza, E.; Rocha, L.A.; Ribeiro, A.R.L.; Vieira, C.; Riviére, J.P.; Pichon, L. Tribocorrosion behaviour of plasma nitrided and plasma nitrided+ oxidised Ti6Al4V alloy. *Surf. Coat. Technol.* **2006**, *200*, 6218–6224. [CrossRef]
15. Mathew, M.T.; Barao, V.A.; Yuan, J.C.; Assunção, W.G.; Sukotjo, C.; Wimmer, M.A. What is the role of lipopolysaccharide on the tribocorrosive behavior of titanium? *J. Mech. Behav. Biomed. Mater.* **2012**, *8*, 71–85. [CrossRef]
16. Fojt, J.; Joska, L.; Málek, J. Corrosion behaviour of porous Ti–39Nb alloy for biomedical applications. *Corros. Sci.* **2013**, *71*, 78–83. [CrossRef]
17. Bayón, R.; Igartua, A.; Gonzalez, J.J.; De Gopegui, U.R. Influence of the carbon content on the corrosion and tribocorrosion performance of Ti-DLC coatings for biomedical alloys. *Tribol. Int.* **2015**, *88*, 115–125. [CrossRef]
18. Albrektsson, T.; Wennerberg, A. Oral implant surfaces: Part 1—Review focusing on topographic and chemical properties of different surfaces and in vivo responses to them. *Int. J. Prosthodont.* **2004**, *17*, 536–543.
19. Albrektsson, T.; Wennerberg, A. Oral implant surfaces: Part 2—Review focusing on clinical knowledge of different surfaces. *Int. J. Prosthodont.* **2004**, *17*, 544–564.
20. Wang, Z.; Zhang, X.; Gu, J.; Yang, H.; Nie, J.; Ma, G. Electrodeposition of alginate/chitosan layer-by-layer composite coatings on titanium substrates. *Carbohydr. Polym.* **2014**, *103*, 38–45. [CrossRef]
21. El-Banna, A.; Bissa, M.W.; Khurshid, Z.; Zohaib, S.; Asiri, F.Y.I.; Zafar, M.S. Surface modification techniques of dental implants. In *Dental Implants*; Woodhead Publishing: Sawston, UK, 2020; pp. 49–58.
22. Anselme, K. Osteoblast adhesion on biomaterials. *Biomaterials* **2000**, *21*, 667–681. [CrossRef] [PubMed]

23. Zhang, B.; Qiu, K.J.; Wang, B.L.; Li, L.; Zheng, Y.F. Surface characterization and cell response of binary Ti-Ag alloys with CP Ti as material control. *J. Mater. Sci. Technol.* **2012**, *28*, 779–784. [CrossRef]
24. Wieckiewicz, M.; Wolf, E.; Richter, G.; Meissner, H.; Boening, K. New concept of polymethyl methacrylate (PMMA) and polyethylene terephthalate (PET) surface coating by chitosan. *Polymers* **2016**, *8*, 132. [CrossRef] [PubMed]
25. Zhang, C.; Hui, D.; Du, C.; Sun, H.; Peng, W.; Pu, X.; Li, Z.; Sun, J.; Zhou, C. Preparation and application of chitosan biomaterials in dentistry. *Int. J. Biol. Macromol.* **2021**, *167*, 1198–1210. [CrossRef]
26. Husain, A.; Al-Samadani, K.H.; Najeeb, S.; Zafar, M.S.; Khurshid, Z.; Zohaid, S.; Qasim, S.B. Chitosan biomaterials for current and potential dental applications. *Materials* **2017**, *10*, 602. [CrossRef]
27. Shukla, S.K.; Mishra, A.K.; Arotiba, O.A.; Mamba, B.B. Chitosan-based nanomaterials: A state-of-the-art review. *Int. J. Biol. Macromol.* **2013**, *59*, 46–58. [CrossRef]
28. Aguilar, A.; Zein, N.; Harmouch, E.; Hafdi, B.; Bornert, F.; Offner, D.; Clauss, F.; Fioretti, F.; Huck, O.; Benkirane-Jessel, N.; et al. Application of Chitosan in Bone and Dental Engineering. *Molecules* **2019**, *24*, 3009. [CrossRef]
29. Hongbin, L.V.; chen, Z.; Yang, X.; Cen, L.; Zhang, X.; Gao, P. Layer-by-layer self-assembly of minocycline-loaded chitosan/alginate multilayer on titanium substrates to inhibit biofilm formation. *J. Dent.* **2014**, *42*, 1464–1472.
30. Renoud, P.; Toury, B.; Benayoun, S.; Attik, G.; Brigitte, G.B. Functionalization of titanium with chitosan via silanation: Evaluation of biological and mechanical performances. *PLoS ONE* **2012**, *7*, e39367. [CrossRef]
31. Lin, M.H.; Wang, Y.H.; Kuo, C.H.; Ou, S.F.; Huang, P.Z.; Song, T.Y.; Chen, Y.C.; Chen, S.T.; Wu, C.H.; Hsueh, Y.H.; et al. Hybrid ZnO/chitosan antimicrobial coatings with enhanced mechanical and bioactive properties for titanium implants. *Carbohydr. Polym.* **2021**, *257*, 117639. [CrossRef]
32. Wang, D.; Chen, C.; Liu, X.; Sheng, X.; Lee, H.-P.; Li, Y. Layer-by-Layer Chitosan/Poly(acrylic acid) Multilayer Coatings for Enhanced Bioactivity of Titanium. *Carbohydr. Polym.* **2014**, *111*, 134–142.
33. Eliaz, N.; Eliyahu, M. Electrochemical Processes of Biomaterials in Human Body Fluids. *Corros. Sci.* **2019**, *165*, 108395.
34. Albrektsson, T.; Wennerberg, A. On Osseointegration in Relation to Implant Surfaces. *Clin. Implant. Dent. Relat. Res.* **2019**, *21*, 4–7. [CrossRef] [PubMed]
35. Caio, Z.; Nakajima, H.; Woldu, M.; Berglund, A.; Bergman, M.; Okabe, T. In vitro corrosion resistance of titanium made using different fabrication methods. *Biomaterials* **1999**, *20*, 183–190. [CrossRef] [PubMed]
36. Ramos, A.P.; Pavarina, A.C.; Dovigo, L.N.; Sanitá, P.V.; Vergani, C.E.; Jorge, J.H.; Machado, A.L. Controlling Growth of Bioactive Films on Titanium Surfaces. *J. Mater. Chem. B* **2015**, *3*, 2455–2464.
37. Decher, G. Fuzzy Nanoassemblies: Toward Layered Polymeric Multicomposites. *Science* **1997**, *277*, 1232–1237. [CrossRef]
38. Shiratori, S.S.; Rubner, M.F. pH-Dependent Thickness Behavior of Sequentially Adsorbed Layers of Weak Polyelectrolytes. *Macromolecules* **2000**, *33*, 4213–4219. [CrossRef]
39. Moreto, J.A.; Gelamo, R.V.; Nascimento, J.P.L.; Taryba, M.; Fernandes, J.C.S. Improving the corrosion protection of 2524-T3-Al alloy through reactive sputtering Nb_2O_5 coatings. *Appl. Surf. Sci.* **2021**, *556*, 149750. [CrossRef]
40. Freitas, L.R.; Gelamo, R.V.; Marino, C.E.B.; Nascimento, J.P.L.; Figueiredo, J.A.M.; Fernandes, J.C.S.; Moreto, J.A. Corrosion behaviour of reactive sputtering deposition niobium oxide-based coating on the 2198-T851 aluminium alloy. *Surf. Coat Technol.* **2022**, *434*, 128197. [CrossRef]
41. Ferreira, M.O.A.; Teixeira, G.T.L.; Leite, N.B.; Gelamo, R.V.; Pinto, H.C.; Aoki, I.V.; Moreto, J.A. Effect of Nb_2O_5 coating on the corrosion resistance of the 7050-T7451 aluminium alloy. *Emergent. Mater.* **2023**, *6*, 2001–2017. [CrossRef]
42. Ferreira, M.O.A.; Mariani, F.E.; Leite, N.B.; Gelamo, R.V.; Aoki, I.V.; de Siervo, A.; Pinto, H.C.; Moreto, J.A. Niobium and carbon nanostructured coatings for corrosion protection of the 316L stainless steel. *Mater. Chem. Phys.* **2024**, *312*, 128610. [CrossRef]
43. Picart, C.; Lavalle, P.; Hubert, P.; Cuisinier, F.J.G.; Decher, G.; Schaaf, P.; Voegel, J.C. Buildup Mechanism for Poly(L-lysine)/Hyaluronic Acid Films onto a Solid Surface. *Langmuir* **2001**, *17*, 7419–7425. [CrossRef]
44. Ramos, A.P.; Pavarina, A.C.; Dovigo, L.N.; Sanitá, P.V.; Vergani, C.E.; Jorge, J.H.; Machado, A.L. Nanoscale Architecture of Layer-by-Layer Films Containing Bioactive Glass Nanoparticles. *Langmuir* **2013**, *29*, 2746–2753.
45. Borges, J.; Mano, J.F. Layer-by-Layer Self-Assembly: A Powerful Tool for the Nanoengineering of Biomaterials. *Chem. Rev.* **2014**, *114*, 8883–8942. [CrossRef]

46. do Nascimento, J.P.L.; Ferreira, M.O.A.; Teixeira, G.T.L.; Slade, N.B.L.; Aoki, I.V.; Moreto, J.A. The Use of POPE Phospholipid as a First-Layer Coating of the Ti-6Al-4V Alloy: Preliminary Studies. *Orbital Electron. J. Chem.* **2024**, *16*, 10–16. [CrossRef]
47. Moreto, J.A.; Marino, C.E.B.; Bose Filho, W.W.; Rocha, L.A.; Fernandes, J.C.S. SVET, SKP and EIS study of the corrosion behaviour of high strength Al and Al–Li alloys used in aircraft fabrication. *Corros. Sci.* **2014**, *84*, 30–41. [CrossRef]